Submitted to

33rd International Conference on High Energy Physics, ICHEP06, July 26 - August 2, 2006, Moscow
Parallel Session **Soft QCD**

Measurement of Deeply Virtual Compton Scattering at HERA II

H1 Collaboration

Abstract

New results on the Deeply Virtual Compton Scattering process $\gamma^* p \to \gamma p$ (DVCS) from the H1 experiment at the ep collider HERA are presented, using data collected during the year 2004 and corresponding to an integrated luminosity of 39.7 pb^{-1}. The DVCS cross section is measured as a function of the photon virtuality, Q^2, the $\gamma^* p$ c.m.s. energy W and differentially in the four momentum transfer squared at the proton vertex, t, in the kinematic range $6.5 < Q^2 < 80$ GeV^2, $30 < W < 140$ GeV and $|t| < 1$ GeV^2. The results are found to be in good agreement with the published H1 measurements and compared to NLO QCD calculations based on Generalized Parton Distributions (GPD) and to predictions from color dipole model.

1 Introduction

Measurements of Deep Inelastic Scattering (DIS), $e\,p \to e\,p\,X$, allow to obtain informations about the structrure of the proton, through the extraction of the parton distribution functions or pdfs. The picture available is nevertheless incomplete, as the pdfs only describe the longitudinal momentum fraction distributions of the constituants of a fast moving proton and do not contain any information about the transverse ones. The study of diffractive exclusive processes in which the proton remains intact after the collision have appeared to be the ideal framework in order to have an insight on this missing transverse information, whose access is made possible through the extraction of the Generalized Partons Distributions or GPDs. Namely, these are the exclusive diffractive vector meson production and the Deeply Virtual Compton Scattering or DVCS process. This latter, which is the hard diffractive scattering of a virtual photon off a proton, $\gamma^* p \to \gamma p$, is represented on figure 1(a). DVCS is of particular interest as it has both a clear experimental signature and is fully calculable in the framework of pertubative Quantum Chromodynamics (pQCD). Unlike the diffractive vector meson production whose theoretical prediction suffers from the uncertainty on the vector meson wave function, the DVCS process, whose diffractive final state consists in a single real photon, is not affected by this lack of knowledge.

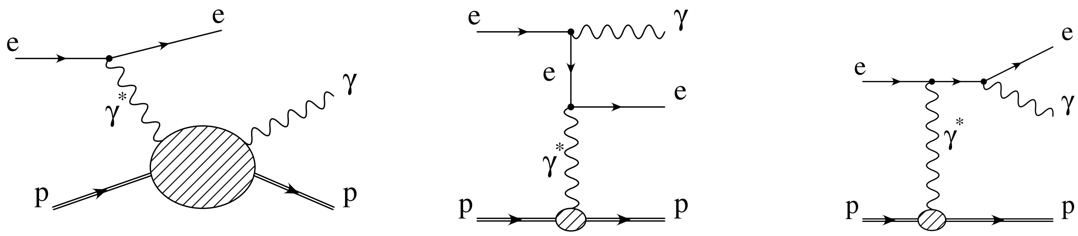

(a) (b) (c)

Figure 1: Deeply Virtual Compton Scattering (a) and Bethe-Heitler processes (b) and (c).

The DVCS process has the same final state as the Bethe-Heitler (BH) process, depicted on figures 1(b) and 1(c). The latter, being purely electromagnetic and involving only elastic proton form factors, is precisely known and can therefore be bin by bin subtracted from the measured signal. The integration over the azimuthal angle indeed ensures that the interference term between the 2 processes vanishes. On the other hand, BH events can be used to study the detector response in the analysis kinematic range.

In the following, new measurements of the Deeply Virtual Compton Scattering are presented, using data collected by the H1 experiment at the ep collider HERA during the year 2004 and corresponding to an integrated luminosity of 39.7 pb^{-1}. The DVCS cross section is measured as a function of the photon virtuality, Q^2, the $\gamma^* p$ c.m.s. energy W and differentially in the four momentum transfer squared at the proton vertex, t, in the kinematic range $6.5 < Q^2 < 80$ GeV^2, $30 < W < 140$ GeV and $|t| < 1$ GeV^2.The results are compared to NLO QCD calculations based on Generalized Parton Distributions (GPD) and to predictions from color dipole model.

2 Theoretical Framework

2.1 Factorization and Generalized Parton Distributions

In the presence of the hard scale $Q^2 \gg M_p^2$ and for low values of the momentum transfer squared at the proton vertex, $|t| \ll Q^2$, the DVCS amplitude factorizes $[1,2]$ into the convolution of coefficient functions, pQCD calculable, and universal functions describing the non-perturbative structure of the proton, the Generalized Parton Distributions or GPDs. Figures 2(a) and 2(b) respectively represent the leading order contribution to DVCS process and one of the next-to-leading order contribution. In order to fulfill the reality of the final state photon, the longitudinal momentum fractions of the outgoing and incoming partons participating to the hard scattering process have to be different, which is encountered for by the introduction of the skewedness ξ. This variable represents half of the difference between the initial and scattered parton's longitudinal momenta, respectively given by $x - \xi$ and $x + \xi$, and is related to the Björken variable x_{bj} by the relation $\xi = x_{bj}/(2 - x_{bj})$. The Generalized Parton Distributions extend the usual pdfs in this non forward region and encode an interpolation between these latters and the elastic form factors of the proton. By this way, they give a unified picture of the proton stucture that contains information about both the longitudinal and transverse distributions of its partons. Unlike the usual pdfs which represent, for a parton in a given state in the infinite momentum frame, a sum of the squared wave functions of this parton over all possible configurations allowing it to be in this state, the GPDs represent the interference between two different wave functions of the parton, associated to different longitudinal momenta $x - \xi$ and $x + \xi$. The GPDs kinematic dependence is in the 3 variables x, ξ and t. The internal variable x is defined in the range $[-1, 1]$, its negative values corresponding to antiquark distributions. The GPDs, as the usual pdfs, are given at a starting scale μ^2 and subsequently Q^2 evolved by QCD evolution equations.

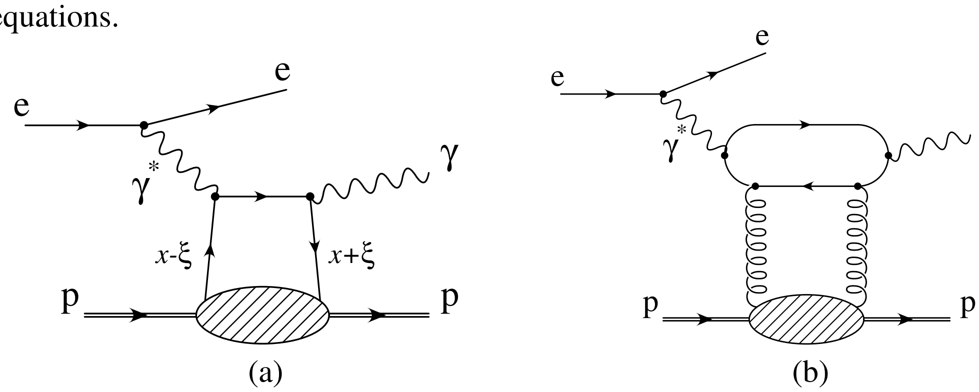

Figure 2: Diagrams contributing to DVCS process at leading order (a) and one of the next-to-leading order contributions (b).

There are four independant GPDs for each type of quark flavors and for gluons, namely $\mathcal{H}^{q,g}(x,\xi,t)$, $\mathcal{E}^{q,g}(x,\xi,t)$, $\widetilde{\mathcal{H}}^{q,g}(x,\xi,t)$ and $\widetilde{\mathcal{E}}^{q,g}(x,\xi,t)$. The $\mathcal{H}^{q,g}(x,\xi,t)$ and $\mathcal{E}^{q,g}(x,\xi,t)$ distributions are present in the unpolarised case as they contain in their definition a sum over the partons helicities, while the $\widetilde{\mathcal{H}}^{q,g}(x,\xi,t)$ and $\widetilde{\mathcal{E}}^{q,g}(x,\xi,t)$ functions, containing in their definition a difference between the right and left handed partons, contribute to the polarised case. The distributions $\mathcal{H}^{q,g}(x,\xi,t)$ and $\widetilde{\mathcal{H}}^{q,g}(x,\xi,t)$ conserve the proton helicity, while $\mathcal{E}^{q,g}(x,\xi,t)$ and

$\widetilde{\mathcal{E}}^{q,g}(x,\xi,t)$ allow for a proton helicity flip, a property which is not present in the framework of ordinary pdfs. In the forward limit $\xi, t \rightarrow 0$, the distributions $\mathcal{E}^{q,g}(x,\xi,t)$ and $\widetilde{\mathcal{E}}^{q,g}(x,\xi,t)$ have thus no equivalent in the usual pdfs approach, while the $\mathcal{H}^{q,g}(x,\xi,t)$ and $\widetilde{\mathcal{H}}^{q,g}(x,\xi,t)$ GPDs reduce to the ordinary non polarised and polarised pdfs respectively [3]. The zero order moments of the GPDs in the variable x are equal to the proton elastic form factors, while the first moment in x of $\mathcal{H}^{q,g}(x,\xi,t)+\mathcal{E}^{q,g}(x,\xi,t)$, evaluated at $t=0$, is equal to twice the total angular momentum of quarks and gluons in the proton, respectively. This latter property is known as the Ji's sum rule [4]. In the DVCS case, the main contribution to the amplitude at low x_{bj} comes from the unpolarised GPDs $\mathcal{H}^{q,g}(x,\xi,t)$ for the quarks and gluons.

The way GPDs evolve with Q^2 is ruled by the value of the x variable w.r.t. that of the skewedness ξ. For $|x| > \xi$, their Q^2 evolution is similar to that induced by the DGLAP equation in the usual pdfs case, and the GPDs are associated to the emission and reabsorption of a quark ($\xi < x < 1$), antiquark ($-1 < x < -\xi$) or gluon. For $|x| < \xi$, the GPDs correspond to the emission of a quark-antiquark or gluons pair and their Q^2 behaviour is alike the ERBL evolution for the meson amplitudes distributions.

2.2 Theoretical Predictions

In the following, data are compared to NLO QCD predictions for the DVCS cross section and to results from the color dipole model. This two approaches are complementary, as the first enables us to test the description pQCD gives of the colorless exchange and to constrain the GPDs inputs, while the latter gives a suitable framework to probe the transition between non perturbative and perturbative regimes.

The NLO QCD calculations have been obtained by Freund and McDermott [5,6] using two different GPDs parametrizations [7]. In the DGLAP region $|x| > \xi$, the usual pdfs $q(x;\mu^2)$ and $g(x;\mu^2)$ from MRST2001 and CTEQ6 are used to parametrize the GPDs $\mathcal{H}^{q,g}(x,\xi,t)$ whose contribution is dominant in the probed low x_{bj} region, while the t dependence is factorized in an exponential behaviour. At the starting scale μ^2, the quark singlet and gluons distributions are thus respectively given by $\mathcal{H}^q(x,\xi,t;\mu^2) = q(x;\mu^2)\, e^{-b|t|}$, $\mathcal{H}^g(x,\xi,t;\mu^2) = xg(x;\mu^2)\, e^{-b|t|}$. In the ERBL region, for $|x| < \xi$, the quark singlet and gluons distributions are parametrized by simple analytic functions, satisfying continuation to the DGLAP region. The Q^2 and ξ dependences are then generated dynamically through the evolution equations, no intrinsic skewedness being included at the starting scale μ^2.

The various color dipole models are based on the time factorization of the DVCS process, which can be seen in the proton rest frame as three subprocesses occuring at well separated time scale. First the incoming virtual photon fluctuates into a $q,\bar{q}$ pair, which subsequently interacts with the proton and then annihilates into the final state real photon. The first and last steps are described by the QED calculable photon wave functions $\Psi_T^{\gamma*}(\vec{r},z,Q^2)$ and $\Psi_T^{\gamma}(\vec{r},z)$ respectively, where $\vec{r}$ represents the transverse size of the dipole, z the longitudinal momentum fraction of the quark, and T refer to the tranverse photon helicity whose s-channel conservation is assumed. The intermediate state corresponding to the interaction between the quak-antiquark pair and the proton is described by a color dipole cross section $\sigma_{dipole}(x_{bj},Q^2,r^2)$, whose parametrization is the main difference between the various color dipole models, each of them assuming an exponential behaviour for the t dependence of the cross section. The model presently compared to the data is due to Favart and Machado [8, 9], who have applied to the DVCS process the saturation model developped by Golec-Biernat and Wüsthoff [10] in order to describe diffractive DIS data, together with the use of a DGLAP evolution for the color dipole cross section, based on the Bartels, Golec-Biernat and Kowalski (BGBK) approach [11].

3 Experimental procedure

3.1 H1 detector

Only a short description of the H1 detector is given here, limited to the detector components relevant for this analysis. A full description may be found in [13]. A right-handed coordinate system is used, with x, y and z axis respectively pointing in the horizontal, vertical and forward or outgoing proton beam directions. The lead scintillating fibre SpaCal calorimeter covers the backward region of the H1 detector, in the angular range $154^\circ < \theta < 174^\circ$, with an energy resolution for electromagnetic showers equal to $\sigma_E/E = 7\,\%/\sqrt{E(\mathrm{GeV})} \oplus 1\,\%$. The liquid argon LAr calorimeter, placed inside a solenoidal magnet, covers the central and forward regions of the H1 detector, in the angular range $4^\circ < \theta < 154^\circ$, with an energy resolution for electromagnetic showers given by $\sigma_E/E = 11\,\%/\sqrt{E(\mathrm{GeV})}$. The backward proportionnal chamber BPC, located in front of the SpaCal, is used to identify and determine the angle of the electron scattered into the backward region. The central tracking detector main components are two cylindrical coaxial drift chambers, the central jet chambers CJC, with wires parallel to the beam direction and angular coverage extending in the range $20^\circ < \theta < 160^\circ$. They ensure the measurement of charged particles transverse momenta, whose trajectories are bended in a 1.15 T magnetic field uniform over the full tracker volume. The forward muon detectors are used to tag hadronic activities at large pseudorapidity $3.2 < \eta < 5.5$, corresponding to the range $3^\circ < \theta < 17^\circ$, occuring in proton dissociation events for which secondary particles interact with the beam pipe. The luminosity measurement is ensured by electromagnetic calorimeters located downstream in the electron beam direction and allowing the determination of the bremsstrahlung events rate.

3.2 Analysis strategy and events selection

These measurements of the DVCS cross section are based on the data collected by the H1 detector during the year 2004, with HERA running with positrons colliding protons of energy 27.5 and 920 GeV respectively, and correspond to an integrated luminosity of 39.7 pb^{-1}. More details about this analysis can be found in [12]. In order to enhance the ratio of DVCS events w.r.t. BH ones, the photon is required to be detected in the forward or central region of the H1 detector, with a transverse momentum $P_T > 2$ GeV, and is identified by an electromagnetic energy shower in the LAr calorimeter together with the absence of associated track in the CJC central tracker. The scattered positron is detected in the backward region, through the presence of an electromagnetic cluster in the SpaCal calorimeter with an energy $E > 20$ GeV. The backward proportionnal chamber BPC is used to determine the electron scattering angle and position by extrapolation into the SpaCal plane, with an angular and spatial resolutions $\sigma_\theta = 0.5$ mrad and $\sigma_R = 0.8$ mm respectively. The CJC acceptance only enables a SpaCal positron track measurement for events with a vituality $Q^2 \gtrsim 25$ GeV^2. For most of the events, the primary vertex position can therefore not be determined and the nominal z vertex position is assumed. To ensure the elastic selection and reduce the proton dissociation background, the presence of other clusters with an energy above the 0.5 GeV noise level is not allowed in the LAr calorimeter, and the absence of hadronic activity at large pseudorapidity is required by a veto condition on the number of hits in the 2 first planes of the forward muon detectors, $N_{hit} < 2$. To reduce radiative corrections influence, the longitudinal momentum balance is required to have values $\sum E - p_z > 45$ GeV, E and p_z respectively denoting the energy and longitudinal momentum of the final state particles, for which the sum runs over. The events fulfilling these conditions belong to the so called DVCS enriched sample, which receives contributions from both DVCS and BH processes for $\sim 60\%$ and $\sim 40\%$ respectively. Their typical signature in the H1 detector is illustrated on figure 3(a).

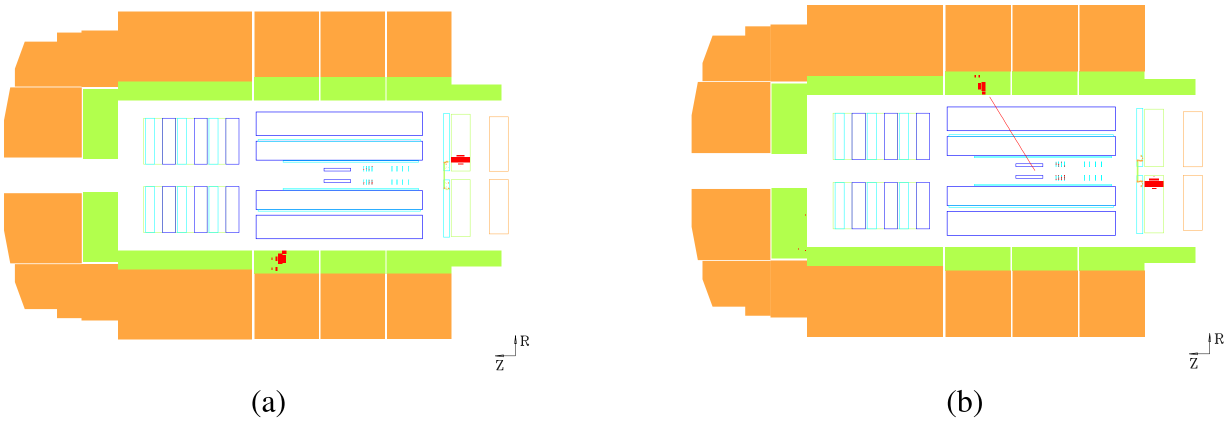

Figure 3: Typical events belonging to the DVCS enriched sample (a) and to the BH control sample (b).

In the aim to study of the detector response, events are also selected with a positron in the forward or central region of the H1 detector, identified by an electromagnetic energy shower in the LAr calorimeter and an associated track in the CJC central tracker, while the photon has to be detected in the SpaCal backward region. The cuts on the particles energy and transverse momentum are taken as above, namely $P_T > 2$ GeV and $E > 20$ GeV for the positron and photon respectively, as well as the elastic selection to reduce the proton dissociation background and the requirement on the longitudinal energy balance. The sample obtained is dominated by BH events contribution and builds up the so-called control sample, whose a typical event is represented on figure 3(b). Besides the understanding of the detector, the BH events are used to calibrate the LAr electromagnetic energy scale in the range $2 < E < 4.5$ GeV, by comparing the calorimeter response with the track momentum CJC measurement.

Events from both samples are kept by the same dedicated trigger, whose level one conditions require an electromagnetic particle candidate to be detected in the SpaCal with an energy $E > 9$ GeV, and level two is a neural network using LAr, SpaCal and CJC informations in order to take its decision. An independant trigger, sharing the same level one conditions but with a topological level two requirement, is used to control and determine the level two neural network trigger efficiency [12].

3.3 Monte Carlo simulation

In order to correct the data for the detector acceptance and resolution and for the initial state photon radiation, Monte Carlo simulations for DVCS, BH and relevant background processes are used. Both elastic and dissociative proton DVCS events are generated by the Monte Carlo generator Milou [14], with a t slope b value of 6.5 and 1.5 GeV-2 respectively. This generator is based on the NLO QCD DVCS cross section obtained by Freund and McDermott [5, 6, 15] and implements initial state photon radiation in the collinear approximation. The elastic and dissociative proton BH events are generated by the Monte Carlo generator Compton 2.20 [16], interfaced to the SOPHIA model package [17] in order to describe low mass hadronisation processes in the inelastic BH events. The elastic diffractive ρ vector meson production and the dilepton production in two photons exchange has been taken into account as background to the BH control sample and have been generated by the Monte Carlo generators DIFFVM [18] and GRAPE [19] respectively. The contribution of elastic ω and ϕ vector mesons production to the DVCS enriched sample, estimated to less than 1% in the 1999-2000 results, have not been taken into account in the present status of the analysis. The events generated are subsequently passed through a detailed simulation of the H1 detector and subject to the same reconstruction procedure and analysis selection as the data. All Monte Carlo expectations are normalized to the luminosity of the data.

3.4 Control plots

The distributions of the energy and polar angle of the scattered positron and final state photon for the DVCS enriched sample, together with those of the coplanarity and positron-photon invariant mass are represented on figures 4. The coplanarity, defined as the difference between the positron and photon azimuthal angles, is related to the p_t balance between the two particles and to the t distribution of the events. The t dependence of the DVCS and BH cross sections respectively reflecting the color and electric charge distribution in the proton, the DVCS t slope is smaller than the BH one, leading to a broadening of the coplanarity distribution for the DVCS events, as can be seen on figure 4(f). The data are shown together with the sum of the Monte Carlo expectations for the elastic and proton dissociative DVCS and BH processes, whose normalizations and shapes give an good description of the signal.

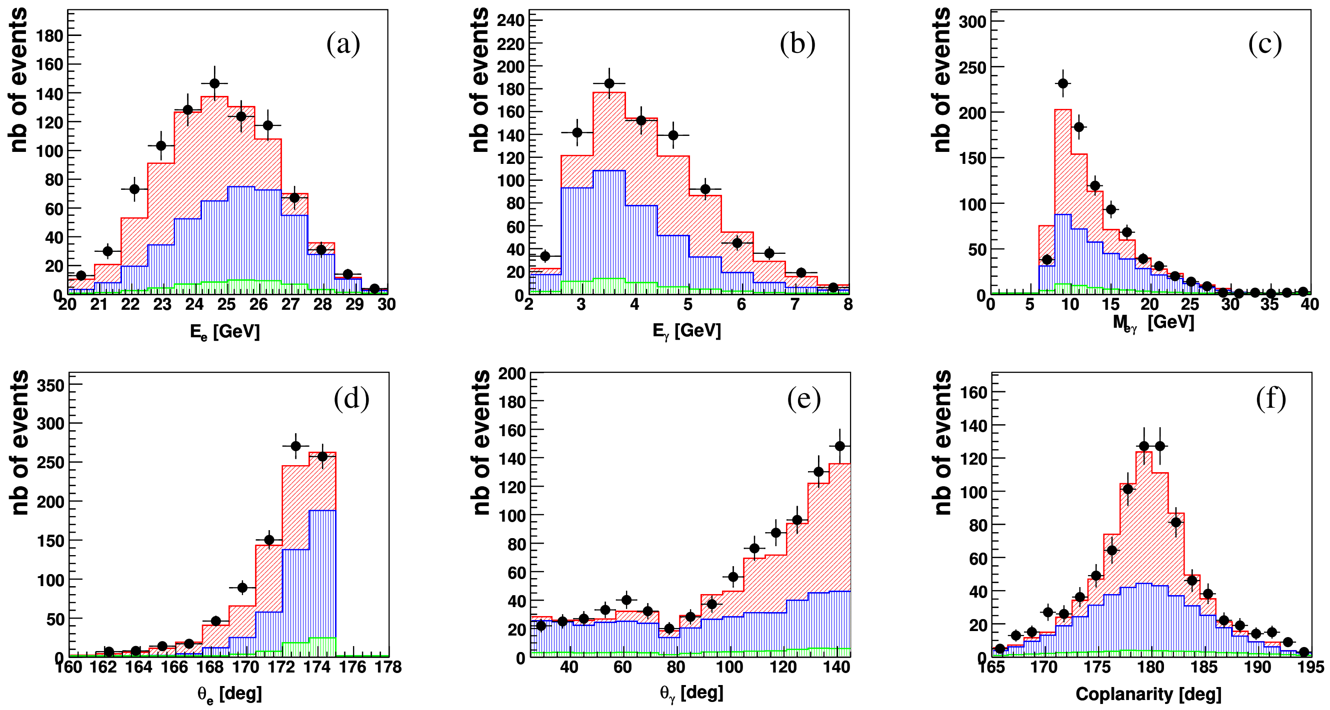

Figure 4: Distributions for the DVCS enriched sample of the energy of the scattered positron (a) and final state photon (b), of the positron-photon invariant mass (c), the polar angle of the scattered positron (d) and photon (e) and the coplanarity (f). The data are compared to the sum of Monte Carlo expectations for proton dissociative DVCS (grey), elastic DVCS (vertically hatched) and elastic and inelastic BH (diagonally hatched).

3.5 Kinematics reconstruction

The event kinematics is reconstructed from the measurement of the positron and photon scattering angles, by the use of the so-called double angle method. This reconstruction procedure is in first approximation independant of the calorimeter calibration and gives for the expression of the Q^2, x_{bj} and W variables:

$$Q^2 = 4E_0^2 \frac{\sin\theta_\gamma(1+\cos\theta_e)}{\sin\theta_\gamma + \sin\theta_e - \sin\theta_e + \theta_\gamma}, \tag{1}$$

$$x_{bj} = \frac{E_0}{E_p} \frac{\sin\theta_\gamma + \sin\theta_e + \sin\theta_e + \theta_\gamma}{\sin\theta_\gamma + \sin\theta_e - \sin\theta_e + \theta_\gamma}, \tag{2}$$

$$W^2 = \frac{Q^2}{x_{bj}}(1 - x_{bj}), \tag{3}$$

where θ_e and θ_γ are the positron and photon scattering angles and E_0 and E_p the nominal positron and proton beam energies. The four momentum transfer squared at the proton vertex, t, is obtained in good approximation from the measurement of the scattered positron and final state photon transverse momenta $\vec{p_t}_e$ and $\vec{p_t}_\gamma$:

$$t \simeq -(\vec{p_t}_e + \vec{p_t}_\gamma)^2. \tag{4}$$

The kinematics variables Q^2, W and t, reconstructed by use of the double angle method and relation 4, are shown on figure 5 for the DVCS enriched sample, for both data and Monte Carlo simulations.

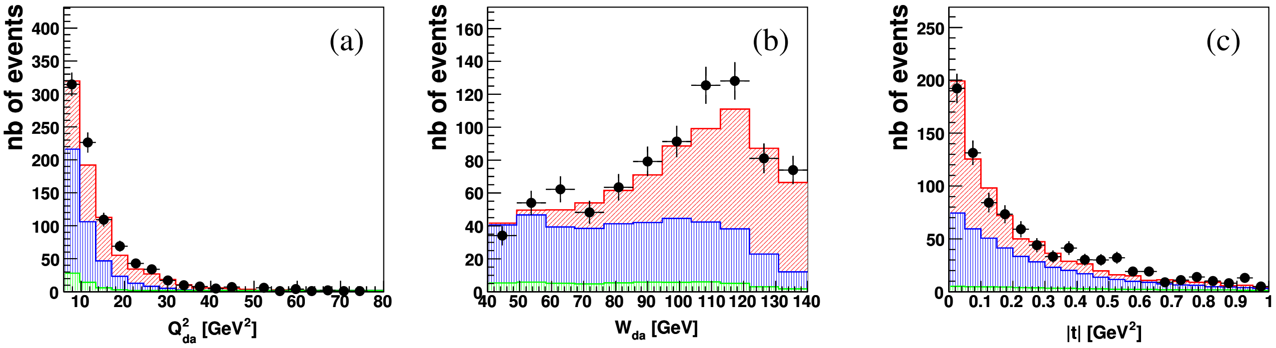

Figure 5: Distributions of kinematic variables for the DVCS enriched sample: the virtuality Q^2 (a), the $\gamma^* p$ c.m.s. energy W (b) and the four momentum transfer squared at the proton vertex t (c). The data are compared to the sum of Monte Carlo expectations for proton dissociative DVCS (grey), elastic DVCS (vertically hatched) and elastic and inelastic BH (diagonally hatched)

3.6 Cross section measurement

To extract the $ep \to ep\gamma$ cross section, the background contributions from elastic BH and proton dissociative BH and DVCS events are subtracted bin by bin using the Monte Carlo expectations given by Milou and Compton 2.20 generators. The data are corrected for trigger efficiency, detector acceptance and initial state photon radiation. The $\gamma^* p \to \gamma p$ cross section is extracted using the equivalent photon approximation:

$$\frac{d^3\sigma[ep \to ep\gamma]}{dQ^2 dy dt}(Q^2, y, t) = \Gamma(Q^2, y) \frac{d\sigma[\gamma^* p \to \gamma p]}{dt}(Q^2, y, t), \tag{5}$$

where Γ is the flux of virtual photons emitted by the incoming positron:

$$\Gamma(Q^2, y) = \frac{\alpha(1 - y + \frac{y^2}{2})}{\pi y Q^2}, \tag{6}$$

with $y = (W^2 + Q^2)/s$ and s the squared positron proton c.m.s. energy. The t dependence of the cross section is subsequently factorized according to an exponential behaviour:

$$\frac{d\sigma[\gamma^* p \to \gamma p]}{dt}(Q^2, y, t) = \left.\frac{d\sigma[\gamma^* p \to \gamma p]}{dt}\right|_{t=0} e^{-b|t|}. \tag{7}$$

The integration of the relation (5) over t enables to write:

$$\frac{d^2\sigma[ep \to ep\gamma]}{dQ^2 dy}(Q^2, y) = \Gamma(Q^2, y)\, \sigma[\gamma^* p \to \gamma p](Q^2, y), \tag{8}$$

where the reduced $\gamma^* p$ cross section is parametrized by the ansatz:

$$\sigma[\gamma^* p \to \gamma p](Q^2, y) = A\, y^a \left(\frac{1}{Q^2}\right)^n. \tag{9}$$

By integrating the left-hand side of relation (8) over Q^2 and y, one obtains:

$$\int_{Q^2_{min}}^{Q^2_{max}} \int_{y_{min}}^{y_{max}} \frac{d^2\sigma[ep \to ep\gamma]}{dQ^2 dy}(Q^2, y)\, dQ^2 dy = \sigma[ep \to ep\gamma] = \frac{C_{tot} N}{L}, \qquad (10)$$

where Q^2_{min}, Q^2_{max}, y_{min} and y_{max} are the boundaries of the bin under consideration, N is the number of events in this bin, L the integrated luminosity of the measurement and C_{tot} the overall correction factor applied to the data. The integration of the right-hand side of relation (8) finally gives the expression of the reduced $\gamma^* p$ cross section at a given bin center (Q^2_0, y_0):

$$\sigma[\gamma^* p \to \gamma p](Q^2_0, y_0) = \frac{C_{tot} N}{L} \frac{1}{D}\, y_0^a \left(\frac{1}{Q^2_0}\right)^n, \qquad (11)$$

with the coefficient D determined by the relation:

$$D = \frac{\alpha}{\pi} \int_{y_{min}}^{y_{max}} \frac{1 - y + \frac{y^2}{2}}{y^{1-a}}\, dy \int_{Q^2_{min}}^{Q^2_{max}} \left(\frac{1}{Q^2}\right)^{n+1} dQ^2. \qquad (12)$$

For the calculation of the $\gamma^* p$ cross section as a function of Q^2, the values of Q^2_{min} and Q^2_{max} are the boundaries of the Q^2 bin under consideration and the integration over y runs over the complete W range of the measurement, while for the determination of the $\gamma^* p$ cross section in W, the values of y_{min} and y_{max} correspond to the boundaries of the considered W bin, the integration over Q^2 running over the full virtuality range of the data. As it is not possible to extract simultaneously the reduced $\gamma^* p$ cross section and the free parameters a and n, the use of an iterative procedure is required. Starting with reasonable values a_0 and n_0, the $\gamma^* p$ cross section is fitted and the extracted Q^2 and y dependences are used as input values for the next iteration step. The Q^2 and W dependences of the slope parameters a and n respectively have been neglected over the range of the measurement.

3.7 Systematic uncertainties

The main sources of systematic errors and the resulting systematic uncertainties affecting the DVCS cross section measurement are:

- the uncertainty on the subtraction of the proton dissociative DVCS background, leading to an uncertainty on the final cross section between 8 and 14 % in the highest $|t|$ bin,
- the uncertainty on the acceptance correction factors, leading to an uncertainty on the final cross section between 2 and 6 % in the highest $|t|$ bin,
- the uncertainty on the determination of the Q^2 and W cross section dependence, leading to an uncertainty on the final cross section between 3 and 6 %,
- the uncertainty on the LAr and SpaCal electromagnetic energy scale, leading to an uncertainty on the final cross section between 2 and 5 %,
- the uncertainty on the scattered positron and final state photon polar angles, respectively 1 and 3 mrad, leading to an uncertainty on the final cross section between 4 and 6 %,
- the uncertainty on the luminosity measurement, of the order of 3 %.

The total systematic error is found to be typically 20 %.

4 Results

The H1 2004 preliminary results are shown together with the published H1 [20] and ZEUS [21] measurements for the DVCS cross sections, in the kinematic range $6.5 < Q^2 < 80$ GeV^2, $30 < W < 140$ GeV and $|t| < 1$ GeV^2. The $\gamma^* p \rightarrow \gamma p$ differential cross section in t is shown on figure 6, for Q^2 = 8 GeV^2 and W = 82 GeV. The H1 2004 preliminary measurements are found to be in agreement with the H1 published ones, while fitting the t dependence of the combined data sample with a function of the form $e^{-b|t|}$ reduces the statistical uncertainty on the t slope, leading to the value $b = 5.83 \pm 0.27 \pm 0.50$ GeV^{-2}, where the first error is statistical, the second systematic.

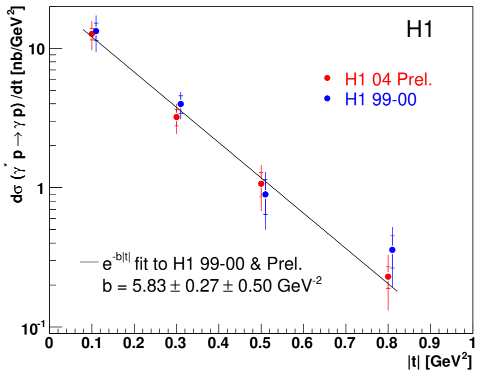

Figure 6: $\gamma^* p \rightarrow \gamma p$ differential cross section in t for Q^2 = 8 GeV^2 and W = 82 GeV. The inner error bars represent the statistical uncertainties, while the full error bars stand for the statistical and systematic uncertainties added quadratically. The exponential fit to the 1999-2000 published and 2004 preliminary H1 results is shown, together with the extracted t slope parameter b.

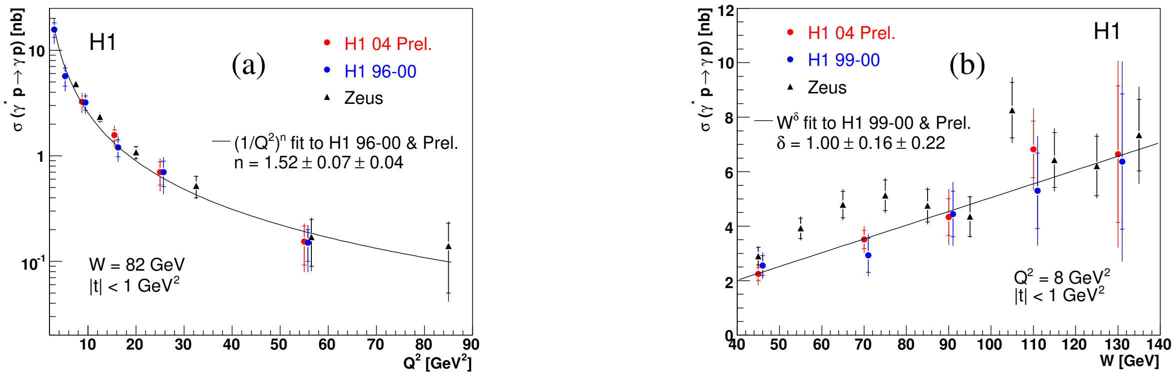

Figure 7: $\gamma^* p \rightarrow \gamma p$ cross section as a function of Q^2 for W = 82 GeV (a) and as a function of W for Q^2 = 8 GeV^2 (b). The inner error bars represent the statistical uncertainties, while the full error bars stand for the statistical and systematic uncertainties added quadratically. The fits to the combined H1 data sample with a function of the form $(1/Q^2)^n$ and W^δ for the Q^2 and W dependence respectively are shown, together with the extracted parameters n and δ.

The $\gamma^* p \rightarrow \gamma p$ cross sections as a function of Q^2 and W, for W = 82 GeV and Q^2 = 8 GeV^2 respectively, are shown on figure 7. Fitting the Q^2 dependence of the combined H1 results with a function of the form $(1/Q^2)^n$ gives $n = 1.52 \pm 0.07 \pm 0.04$, while fitting the W dependence with a function of the form W^δ gives $\delta = 1.00 \pm 0.16 \pm 0.22$, with the first error statistical and the second systematic. This value of δ, comparable to that of diffractive J/Ψ vector meson production [22, 23], indicates the presence of the hard regime. The H1 2004 preliminary measurements are found to be in very good agreement with H1 published results and are compatible with ZEUS measurements, while the H1 combined fit reduces the statistical uncertainty on the slopes n and δ.

On figure 8, the $\gamma^* p \rightarrow \gamma p$ cross sections in function of Q^2 and W are compared to the NLO QCD predictions by Freund and McDermott [5, 6], for two different parametrizations of the usual pdfs, MRST 2001 and CTEQ6, used as input for the GPDs in the DGLAP region. The QCD predictions are in good agreement with the data and show sensitivity to the pdfs input used for the GPDs parametrization. The uncertainty on the normalization is reduced by the measurement of the t slope parameter b, whose uncertainty is reflected by the error band associated to the different curves. The comparison between the data and the theoretical calculations shows no need for intrinsic skewedness.

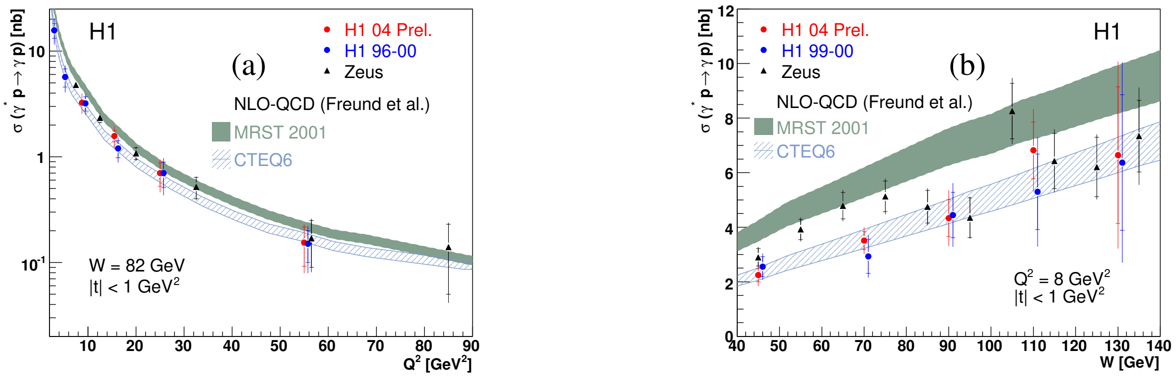

Figure 8: $\gamma^* p \rightarrow \gamma p$ cross section as a function of Q^2 for W = 82 GeV (a) and W for Q^2 = 8 GeV^2 (b). The H1 2004 preliminary measurements are shown together with the published H1 and ZEUS results and compared to NLO QCD predictions by Freund and McDermott using MRST 2001 and CTEQ6 pdfs. The error band associated to the different curves corresponds to the uncertainty on the t slope measurement.

The figure 9 compares the $\gamma^* p \rightarrow \gamma p$ cross sections in function of Q^2 and W to the color dipole model predictions by Favart and Machado [8,9]. This model is found to give a reasonable description of the data, while the contribution of large dipole sizes, whose interactions with the proton are mainly soft, is maybe overestimated, as could indicate the different W dependence between the model and the data. The error band associated to the different curves corresponds to the uncertainty on the t slope measurement.

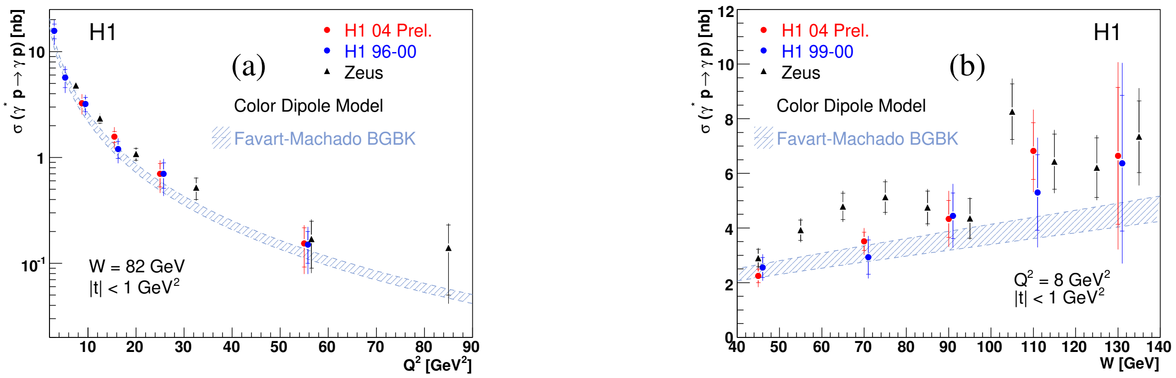

Figure 9: $\gamma^* p \rightarrow \gamma p$ cross section as a function of Q^2 for W = 82 GeV (a) and W for Q^2 = 8 GeV^2 (b). The H1 2004 preliminary measurements are shown together with the published H1 and ZEUS results and compared to the predictions from color dipole model by Favart and Machado. The error band associated to the different curves corresponds to the uncertainty on the t slope measurement.

5 Conclusion

A new measurement of the DVCS cross sections, based on the data collected during the year 2004 of the HERA II period, has been presented in the kinematic range $6.5 < Q^2 < 80$ GeV^2, $30 < W < 140$ GeV and $|t| < 1$ GeV^2. The H1 2004 preliminary results are found to be in very good agreement with the H1 published ones and are compatible with the ZEUS measurement, while the NLO QCD and color dipole model predictions give a good description of the data, both in shape and normalization. The fits to the combined H1 results have allowed to decrease the statistical uncertainties on the slopes b, n and δ characterizing the differential $\gamma^* p \rightarrow \gamma p$ cross section in t and the $\gamma^* p \rightarrow \gamma p$ cross sections in Q^2 and W respectively. Their values are respectively $b = 5.83 \pm 0.27 \pm 0.50$ GeV^{-2}, $n = 1.52 \pm 0.07 \pm 0.04$ and $\delta = 1.00 \pm 0.16 \pm 0.22$.

6 Acknowledgements

We are grateful to the HERA machine group whose outstanding efforts have made and continue to make this experiment possible. We thank the engineers and technicians for their work in constructing and now maintaining the H1 detector, our funding agencies for financial support, the DESY technical staff for continual assistance and the DESY directorate for the hospitality which they extend to the non-DESY members of the collaboration.

References

[1] J. C. Collins and A. Freund, "Proof of factorization for deeply virtual Compton scattering in QCD", Phys. Rev. D **59** (1999) 074009 [hep-ph/9801262].

[2] A. V. Radyushkin and C. Weiss, "DVCS amplitude at tree level: Transversality, twist-3, and factorization", Phys. Rev. D **63** (2001) 114012 [hep-ph/0010296].

[3] M. Diehl, "Generalized parton distributions", Phys. Rept. **388** (2003) 41, DESY-THESIS-2003-018 [hep-ph/0307382].

[4] P. Hoodbhoy, X. D. Ji and W. Lu, "Implications of color gauge symmetry for nucleon spin structure" Phys. Rev. D **59** (1999) 074010 [hep-ph/9808305].

[5] A. Freund and M. F. McDermott, "A next-to-leading order analysis of deeply virtual Compton scattering", Phys. Rev. D **65** (2002) 091901 [hep-ph/0106124].

[6] A. Freund and M. McDermott, "A detailed next-to-leading order QCD analysis of deeply virtual Compton scattering observables", Eur. Phys. J. C **23** (2002) 651 [hep-ph/0111472].

[7] A. Freund, M. McDermott and M. Strikman, "Modelling generalized parton distributions to describe deeply virtual Compton scattering data", Phys. Rev. D **67** (2003) 036001 [hep-ph/0208160].

[8] L. Favart and M. V. T. Machado, "Deeply virtual Compton scattering and saturation approach", Eur. Phys. J. C **29** (2003) 365 [hep-ph/0302079].

[9] L. Favart and M. V. T. Machado, "QCD evolution and skewedness effects in color dipole description of DVCS", Eur. Phys. J. C **34** (2004) 429 [hep-ph/0402018].

[10] K. Golec-Biernat and M. Wusthoff, "Saturation in diffractive deep inelastic scattering", Phys. Rev. D **60** (1999) 114023 [hep-ph/9903358].

[11] J. Bartels, K. Golec-Biernat and H. Kowalski, "DGLAP evolution in the saturation model", Acta Phys. Polon. B **33** (2002) 2853 [hep-ph/0207031].

[12] B. Roland, "Measurement of Deeply Virtual Compton Scattering at HERA II", Doctoral Thesis, Université Libre de Bruxelles, in litterature.

[13] I. Abt *et al.* [H1 Collaboration], "The Tracking, calorimeter and muon detectors of the H1 experiment at HERA ", Nucl. Instrum. Meth. A **386** (1997) 310 and 348.

[14] E. Perez, L. Schoeffel and L. Favart, "MILOU: A Monte-Carlo for deeply virtual Compton scattering", DESY-04-228 [hep-ph/0411389].

[15] A. Freund, "A detailed QCD analysis of twist-3 effects in DVCS observables", Phys. Rev. D **68** (2003) 096006 [hep-ph/0306012].

[16] A. Courau, S. Kermiche, T. Carli and P. Kessler, "Quasireal QED Compton Monte Carlo", *Proceedings of the Workshop on Physics at HERA*, eds. W. Buchmüller, G. Ingelman, Vol. 2: p. 902, Hamburg 1991.

[17] V. Lendermann, "Measurement of the QED Compton scattering cross section with the H1 detector at HERA", DESY-THESIS-2002-004.

[18] B. List and A. Mastroberardino, "DIFFVM: A Monte Carlo generator for diffractive processes in ep scattering", *Proceedings of the DESY workshop on Monte Carlo Generators for HERA Physics*, eds. A. T. Doyle, G. Grindhammer, G. Ingelman and H. Jung, DESY-PROC-1999-02, p. 396.

[19] T. Abe,"GRAPE-Dilepton (Version 1.1): A generator for dilepton production in e p collisions", Comput. Phys. Commun. **136** (2001) 126 [hep-ph/0012029].

[20] A. Aktas *et al.* [H1 Collaboration], "Measurement of deeply virtual Compton scattering at HERA", Eur. Phys. J. C **44** (2005) 1 [hep-ex/0505061].

[21] S. Chekanov *et al.* [ZEUS Collaboration], "Measurement of deeply virtual Compton scattering at HERA", Phys. Lett. B **573** (2003) 46 [hep-ex/0305028].

[22] C. Adloff *et al.* [H1 Collaboration], "Charmonium production in deep inelastic scattering at HERA", Eur. Phys. J. C **10** (1999) 373 [hep-ex/9903008].

[23] S. Chekanov *et al.* [ZEUS Collaboration], "Exclusive photoproduction of J/psi mesons at HERA", Eur. Phys. J. C **24** (2002) 345 [hep-ex/0201043].